



Ultrafast laser-inscribed mid-infrared transmission gratings in IG2: modelling and high-resolution spectral characterization

HELEN L BUTCHER,¹ DAVID LEE,² RICHARD BROWNSWORD,¹ DAVID G MACLACHLAN,³ ROBERT R THOMSON,³ AND DAMIEN WEIDMANN^{1,*}

¹Space Science and Technology Department (RAL Space), STFC Rutherford Appleton Laboratory, Harwell Campus, Didcot, OX11 0QX, UK

²Science and Technology Facilities Council, UK Astronomy Technology Centre, Blackford Hill, Edinburgh, EH9 3HJ, UK

³Scottish Universities Physics Alliance (SUPA), Institute of Photonics and Quantum Sciences, School of Engineering and Physical Sciences, David Brewster Building, Heriot Watt University, Edinburgh, EH14 4AS, UK

*damien.weidmann@stfc.ac.uk

Abstract: The ultrafast laser inscription technique was used to fabricate mid-infrared volume gratings in the bulk of chalcogenide glass IG2 ($\text{Ge}_{33}\text{As}_{12}\text{Se}_{55}$). These gratings are spectrally characterized using a Fourier transform infrared spectrometer, by measuring the transmission spectrum over the entire transmission band of the IG2 substrate. The gratings exhibit first order diffraction across the entire 2–5 μm spectral band, with the specific transmission band tuned by changing the angle of incidence. Higher diffraction orders are also observed. High-resolution spectral data is presented alongside detailed modelling and analysis. This work provides the basis for future design of mid-infrared transmission gratings; ULI provides a low-cost, robust alternative to mid-infrared reflection gratings, with the added capability to engineer the grating response to a specific application.

Published by The Optical Society under the terms of the [Creative Commons Attribution 4.0 License](https://creativecommons.org/licenses/by/4.0/). Further distribution of this work must maintain attribution to the author(s) and the published article's title, journal citation, and DOI.

OCIS codes: (050.0050) Diffraction and gratings; (050.7330) Volume gratings; (050.6875) Three-dimensional fabrication; (140.3390) Laser materials processing.

References and links

1. P. Léna, D. Rouan, F. Lebrun, F. Mignard, and D. Pelat, *Observational Astrophysics* (Springer-Verlag Berlin Heidelberg, 2012).
2. M. A. Kenworthy and P. M. Hinz, "Spectrophotometry with a transmission grating for detecting faint occultations," *Publ. Astron. Soc. Pac.* **115**(805), 322–333 (2003).
3. D. Crisp, H. R. Pollock, R. Rosenberg, L. Chapsky, R. A. M. Lee, F. A. Oyafuso, C. Frankenberg, C. W. O'Dell, C. J. Bruegge, G. B. Doran, A. Eldering, B. M. Fisher, D. Fu, M. R. Gunson, L. Mandrake, G. B. Osterman, F. M. Schwandner, K. Sun, T. E. Taylor, P. O. Wennberg, and D. Wunch, "The on-orbit performance of the orbiting carbon observatory 2 (OCO-2) instrument and its radiometrically calibrated products," *Atmos. Meas. Tech.* **10**, 59–81 (2017).
4. G. Tinetti, T. Encrenaz, and A. Coustenis, "Spectroscopy of planetary atmospheres in our Galaxy," *Astron. Astrophys. Rev.* **21**(63), 1–65 (2013).
5. D. Jakovels, J. Filipovs, G. Erins, and J. Taskovs, "Airborne hyperspectral imaging in the visible-to-mid wave infrared spectral range by fusing three spectral sensors," *Proc. SPIE* **9245**, 92450P (2014).
6. B. Stuart, *Biological Applications of Infrared Spectroscopy* (Wiley, 1997).
7. H. Amrania, A. P. McCrow, M. R. Matthews, S. G. Kazarian, M. K. Kuimova, and C. C. Phillips, "Ultrafast infrared chemical imaging of live cells," *Chem. Sci. (Camb.)* **2**(1), 107–111 (2011).
8. C. Palmer and E. Loewen, *Diffraction Grating Handbook* (Newport Corporation, 2014).
9. J. A. Arns, W. S. Colburn, and S. C. Barden, "Volume phase gratings for spectroscopy, ultrafast laser compressors, and wavelength division multiplexing," *Proc. SPIE* **3779**, 313–323 (1999).
10. N. Nikonov, S. Ivanov, V. Dubrovin, and A. Ignatiev, "New Photo-Thermo-Refractive Glasses for Holographic Optical Elements: Properties and Applications," in *Holographic Materials and Optical Systems*, I. Naydenova ed. (InTech, 2017).

11. T. Ribauto, B. Passmore, K. Freitas, E. A. Shaner, J. G. Cederberg, and D. Wasserman, "Loss mechanisms in mid-infrared extraordinary optical transmission gratings," *Opt. Express* **17**(2), 666–675 (2009).
12. S. Krivoslykov, "Holographic recording of infrared diffractive optics based on ZnSe material," *Appl. Opt.* **54**(12), 3569–3575 (2015).
13. K. M. Davis, K. Miura, N. Sugimoto, and K. Hirao, "Writing waveguides in glass with a femtosecond laser," *Opt. Lett.* **21**(21), 1729–1731 (1996).
14. R. R. Thomson, R. J. Harris, T. A. Birks, G. Brown, J. Allington-Smith, and J. Bland-Hawthorn, "Ultrafast laser inscription of a 121-waveguide fan-out for astrophotonics," *Opt. Lett.* **37**(12), 2331–2333 (2012).
15. N. Jovanovic, P. G. Tuthill, B. Norris, S. Gross, P. Stewart, N. Charles, S. Lacour, M. Ams, J. S. Lawrence, A. Lehmann, C. Niel, J. G. Robertson, G. D. Marshall, M. Ireland, A. Fuerbach, and M. J. Withford, "Starlight demonstration of the Dragonfly instrument: an integrated photonic pupil-remapping interferometer for highcontrast imaging," *Mon. Not. R. Astron. Soc.* **427**(1), 806–815 (2012).
16. S. Minardi, F. Dreisow, M. Gräfe, S. Nolte, and T. Pertsch, "Three-dimensional photonic component for multichannel coherence measurements," *Opt. Lett.* **37**(15), 3030–3032 (2012).
17. D. G. MacLachlan, R. J. Harris, I. Gris-Sánchez, T. J. Morris, D. Choudhury, E. Gendron, A. G. Basden, I. Spaleniak, A. Arriola, T. A. Birks, J. R. Allington-Smith, and R. R. Thomson, "Efficient photonic reformatting of celestial light for diffraction-limited spectroscopy," *Mon. Not. R. Astron. Soc.* **464**(4), 4950–4957 (2017).
18. J. Tepper, L. Labadie, R. Diener, S. Minardi, J. U. Pott, R. Thomson, and S. Nolte, "Integrated optics prototype beam combiner for long baseline interferometry in the L and M bands," *Astron. Astrophys.* **602**, A66 (2017).
19. D. G. MacLachlan, R. R. Thomson, C. R. Cunningham, and D. Lee, "Mid-infrared volume phase gratings manufactured using ultrafast laser inscription," *Opt. Mater. Express* **3**(10), 1616–1623 (2013).
20. D. G. MacLachlan, D. Choudhury, A. Arriola, C. Cunningham, R. R. Thomson, A. Kirkham, and D. Lee, "Developing ultrafast laser inscribed volume gratings," *Proc. SPIE* **9151**, 91511H (2014).
21. M. N. Polyanskiy, "Refractive index database," <https://refractiveindex.info/?shelf=glass&book=VITRON-IG&page=IG2>.
22. D. Lee, D. G. MacLachlan, H. L. Butcher, R. A. Brownsword, D. Weidmann, C. R. Cunningham, H. Schnetler, and R. R. Thomson, "Mid-infrared transmission gratings in chalcogenide glass manufactured using ultrafast laser inscription," *Proc. SPIE* **9912**, 99122X (2016).
23. M. Ams, G. D. Marshall, and M. J. Withford, "Study of the influence of femtosecond laser polarisation on direct writing of waveguides," *Opt. Express* **14**(26), 13158–13163 (2006).
24. D. Fluckiger, "About GSolver," <http://www.gsolver.com/about/index.html>.
25. J. Loicq, L. M. Venancio, Y. Stockman, and M. P. Georges, "Performances of volume phase holographic grating for space applications: study of the radiation effect," *Appl. Opt.* **52**(34), 8338–8346 (2013).
26. P. Vojtíšek, M. Květoň, and I. Richter, "Effective spectral dispersion of refractive index modulation," *J. Opt.* **19**(4), 045603 (2017).

1. Introduction

Diffraction gratings are one of the main optical tools used to carry out dispersive spectrometry. The middle infrared (mid-IR) spectral region, and particularly the 3–5 μm atmospheric transparency window, underpins numerous multispectral or hyperspectral applications. Indeed, not only does the 3–5 μm window exhibit limited spectral interference from water vapor, but it also coincides with "fingerprint" ro-vibrational bands in which many molecules can be spectrally characterized, and specifically the C-H bond. In astronomy and space sciences, mid-IR transmission gratings contribute to the development of spectrometers able to remotely analyze composition, velocity and temperature, amongst other characteristics, of celestial bodies and interstellar medium [1,2]. In Earth and (exo-)planetary observation, mid-IR spectrometers play a key role in the remote sounding of atmospheric composition [3,4] and land or ocean characterization [5]. In biophotonics, mid-IR spectrometers have numerous applications in fluid analysis, including analysis of exhaled breath composition [6]. Mid-IR spectroscopy is used alongside traditional microscopy techniques for medical imaging [7]. In applications related to light molecular gas analysis, gratings with high spectral resolution and good out-of-band extinction are particularly sought after to provide high specificity.

While mid-IR reflection gratings are the most widely used in spectrometers, optical configurations would benefit from the design flexibilities afforded by transmission gratings, including reduced polarization sensitivity and the convenience of an unfolded beam path. However, suitable materials and current manufacturing techniques limit the availability and durability of mid-IR transmission gratings. Commercially available transmission gratings are typically fabricated via two methods; replication or holographic patterning [8,9]. In

replication, a 'master' ruled grating is fabricated and the impression of this grating transferred to an epoxy layer on a transmissive material. The epoxy used is typically a polymer with low refractive index ($n \approx 1.6$) compared with those of typical mid-IR transmitting materials ($n > 2$). These transmission gratings are lossy in the mid-IR due to inherent material transmission characteristics in this region, and exhibit high polarization sensitivity. Holographic patterning involves creating an interference pattern, which is used to define grating lines on a material. The material most frequently used for this is dichromated gelatin, which does not transmit beyond $2.2 \mu\text{m}$, limiting the practical application of this grating in the mid-IR. In addition, the size of the interference pattern limits the size of the grating, further reducing practical use with large aperture. Gratings manufactured using both methods are extremely delicate as the index-modulation structure is in a soft, accessible surface material; extreme care must be taken not to damage the grating structure during use. Holographic patterning can also be employed within photo-thermo-refractive glass [10], creating a more robust optical component, but the silicate substrate with cut-off at $2.5 \mu\text{m}$ again precludes use as a transmission grating in the mid-IR. Recent developments in transmission grating technology have employed sub-wavelength microstructured films on mid-IR transmissive substrates [11], and low-intensity photomodification of polycrystalline semiconductors [12]. Whilst these advances have improved the performance of mid-IR transmission gratings, these are not yet commercially available, and the former still suffers from the delicacy that results from surface patterning.

An alternative transmission grating fabrication technique is ultrafast laser inscription (ULI). Owing to the high fluence deposited within a dielectric material by a focused incident laser beam, ULI creates a local structural modification in the bulk material. Under the correct conditions, irradiation of a substrate material with ultrashort laser pulses causes a combination of non-linear processes that alter the local material structure, resulting in a modification of the local refractive index of the material [13]. The ability to create custom three-dimensional structures in a variety of materials has led to the technique being investigated for use in a variety of applications in astronomy [14–18]. Mid-IR optical materials suitable for ULI include gallium lanthanum sulphide (GLS) chalcogenide glass [19]; the first demonstration of an ULI volume phase transmission grating in the infrared was in GLS, and showed promising performance in the near- to short-wave infrared, out to $2.6 \mu\text{m}$ [20].

Volume gratings have significant optical advantages over alternative surface relief transmission gratings, in terms of both higher diffraction efficiency and also greater spectral selectivity. The specific advantage of a ULI volume grating is that it is fully embedded within a material, eliminating the delicacy of traditional surface relief transmission gratings, and therefore delivering a highly rugged component. ULI refractive index modification is possible in a variety of materials, thus extending the choice to spectral regions that are difficult to access using conventional fabrication techniques. In addition to increased material versatility, the single-beam direct-writing ULI technique allows tailoring of the spectral response function through inscription of engineered index-modulation structures. Bulk inscription could be made directly into optical components such as lenses or prisms, hence combining optical functions. Finally, the technique allows rapid prototyping of structures for iterative design and test.

Developing ULI volume gratings suitable for the mid-IR requires either: increasing the overall thickness of the grating structure within the material; or increasing the refractive index contrast caused by ULI. The former involves longer fabrication time that may jeopardize the grating efficiency, due to temporal instability of the fabrication equipment on spatial scales on the same order as the inscription spot size. Increasing the refractive index contrast means increasing the pulse energy during manufacture. However, the physical properties of the material limit the pulse energy that can be applied before damage occurs, and therefore the

refractive index modification that can be achieved. As a result, a more promising approach would be the investigation of alternative materials.

In this work, we are characterizing and analyzing the use of chalcogenide glass IG2 ($\text{Ge}_{33}\text{As}_{12}\text{Se}_{55}$) [21] for volume grating inscription. IG2 is a commercial glass commonly used in thermal imaging, and has been demonstrated to exhibit greater refractive index modification than GLS when similar ULI parameters were used [22]. This paper briefly describes the fabrication of devices, the optimization for mid-IR wavelength (3 μm), and presents high-resolution spectral characterization of a test grating by Fourier transform spectrometry. The characterization of the measured IG2 grating response is interpreted through detailed theoretical modelling to produce quantitative estimates of refractive index modification, and period structure.

2. Fabrication and optimization of volume gratings

The ULI system used to manufacture volume gratings in IG2 has been described elsewhere [19]. In summary, the source is a fiber laser (Menlo BlueCut), which supplied ~ 355 fs pulses at 1030 nm, with 500 kHz repetition rate. The pulse energy was set to 13 nJ, and the polarization state was circular [23]. The laser field was focused into the material sample using an objective lens with numerical aperture (NA) of 0.4, forming a laser beam waist of approximately 1 μm at the focal point. To allow three-dimensional motion with respect to the beam focus, the sample is mounted on a three-axis air-bearing translation system (Aerotech ABL1000) interfaced to a LabView control program.

The first step towards optimized mid-IR gratings was to conduct a parameter study of inscription pulse energy, using near-infrared (NIR) gratings to ease the characterization, assuming the wavelength dependence with resulting refractive index modification to be insignificant. To that end, fourteen 3 mm square gratings were inscribed in a 25 mm diameter, 1 mm thick IG2 disc. Grating lines were inscribed within the glass, starting at a depth of approximately 260 μm . The grating spatial period was 3 μm , with a total of 1000 periods. Grating lines were formed by translating the sample at 10 mm/s. The gratings were formed of 15 layers separated by a vertical stage movement of 1.7 μm , equivalent to an overall grating optical thickness of ~ 66 μm within the material at the inscription wavelength due to the refractive index of IG2, $n \approx 2.591$ [21].

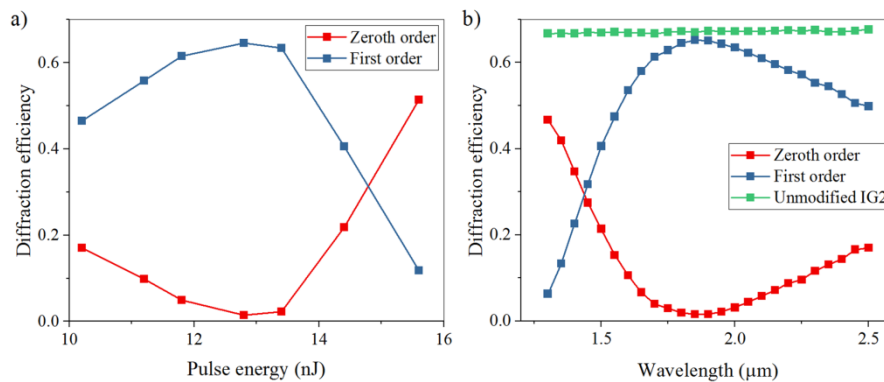


Fig. 1. (a) Plot of absolute zeroth and first order diffraction efficiencies for 15 layer IG2 gratings with varying inscription pulse energy. Diffraction efficiency was measured at 1.9 μm , with the angle optimized for maximum first order efficiency. b) Plot of first and zeroth order diffraction efficiency of the 12.8 nJ, 15 layer grating, as a function of wavelength. Grating transmission was measured under Littrow conditions. The transmission of an area of unmodified material is shown for reference.

The spectral properties of the test gratings were analyzed in the NIR on a similar setup to that described in [19], comprising a white light source, an order sorting filter, a grating

monochromator, an optical fiber, a collimating lens and a Xenics Xeva-2.5-320 infrared camera. The monochromator was set to a wavelength of 1.9 μm , and the 2 mm beam from the white light source was positioned on the center of each grating in turn. The angle of incidence (AOI) was changed to maximize the diffraction to the first order, and both first and zeroth order diffraction efficiency was measured. This was repeated for all test gratings in order to derive the NIR diffraction efficiency as a function of inscription pulse energy, as shown in Fig. 1(a).

For pulse energies below 8 nJ, ULI modification was insignificant, and for pulse energies above 30 nJ ULI caused irreversible damage to the sample. The optimum pulse energy maximizing the first order diffraction efficiency was found to be 12.8 nJ, and was retained for mid-IR grating inscription.

The test grating inscribed at 12.8 nJ, was further characterized in the NIR under Littrow illumination conditions to derive the maximum first order diffraction efficiency as a function of wavelength, as shown in Fig. 1(b) (blue solid line). The transmission of an unmodified region of the sample was also measured. At the optimum wavelength, 1.85 μm , the first order diffraction efficiency was 65%, which is close to the measured 67% transmission efficiency of the bulk material limited by Fresnel reflection losses (green dots and line). With application of a suitable anti-reflection coating, as previously demonstrated for a GLS grating [20], the first order diffraction efficiency could be expected to reach 96% at these wavelengths.

For a given refractive index contrast, extension of IG2 volume gratings to longer wavelengths requires increasing the grating thickness. To understand and characterize the implications of doing so, additional gratings were fabricated consisting of 10 and 22 layers. These were characterized in the NIR as described above, and the summary of their first order diffraction efficiencies is provided in Fig. 2(a). The highest peak diffraction efficiency occurs for the 15 layer grating. This is consistent with previous observations in GLS [19], and is thought to be due to a depth dependent change in refractive index modification.

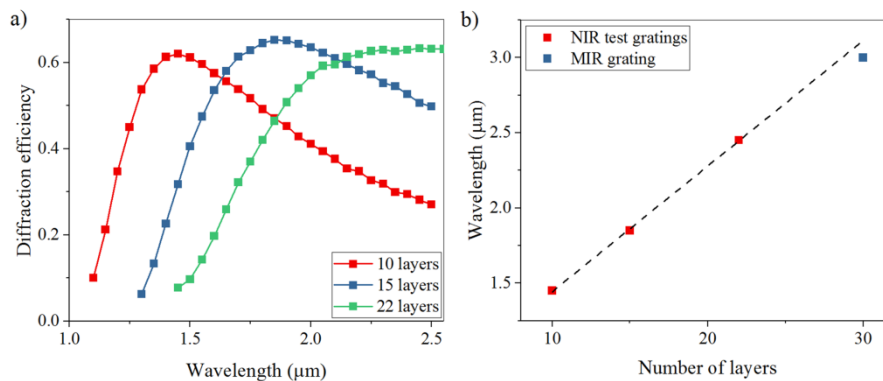


Fig. 2. (a) First order diffraction efficiency vs. wavelength for three different NIR grating thicknesses, measured in the Littrow configuration. (b) Corresponding optimum first order diffraction wavelength vs. grating thickness, for the NIR test gratings (red square) and the thicker MIR grating (blue). The linear fit (dashed) used to interpolate the design wavelength, calculated from the number of grating layers in the NIR (red), is also shown.

The upper limit of the NIR measurement apparatus was 2.5 μm . Nevertheless, by plotting the peak first order diffraction efficiency wavelength against the number of inscribed layers, and assuming a linear relationship as shown in Fig. 2(b), the test NIR gratings characterization is used to derive an estimate of the mid-IR devices' thickness.

The mid-IR grating was inscribed over a 6 mm square area in the IG2 disk, and the number of layers was chosen to target optimum first order diffraction efficiency close to 3 μm . Grating lines were inscribed within the glass, starting at a depth of approximately 280

μm . The grating was formed of 30 layers to achieve an optical thickness of $\approx 128 \mu\text{m}$ at $3 \mu\text{m}$ ($n = 2.5181$ at $3 \mu\text{m}$ [21]), and had a grating spatial period of $3 \mu\text{m}$ with a total of 2000 periods. A photograph of the fabricated grating is shown in Fig. 3(a), for which an incandescent lamp was used along with a standard color CMOS camera.

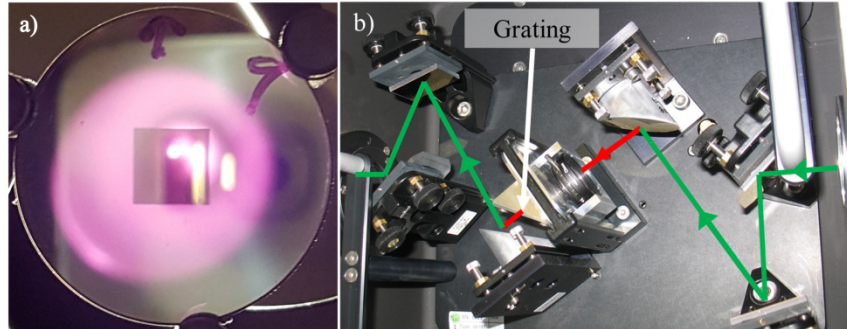


Fig. 3. (a) Image of the fabricated grating (square section) in the IG2 substrate (round disc). (b) Measurement setup, consisting of collimated beam accessory within the sample compartment of the Bruker Vertex 80v. Collimated beam section shown in red. Arrowheads indicate beam trajectory through sample compartment. The grating mount shown in the center is set up for static angle measurement; this can be replaced with a rotation mount for discrete angle measurement.

3. Mid-IR grating characterization

Grating characterization in the mid-IR was undertaken using a Bruker Vertex 80v Fourier Transform Spectrometer (FTS). The grating was characterized in transmission mode, using an unpolarized, collimated beam of spectrally broadband radiation. The layout inside the FTS is shown in Fig. 3(b). The zeroth order transmission was measured, which is the component of radiation that travels straight through the grating, as per [22]. The beam falling upon the sample grating was apertured by a mask so that only the grating structure was illuminated, hence cancelling measurement artifact from transmission through the bulk IG2 component. The grating sample was installed on a rotation stage to vary the incoming beam AOI at the IG2 surface.

Prior to measurement, the FTS settings were optimized. The glowbar broadband source and KBr beamsplitter allowed spectral characterization between 1.5 and $20 \mu\text{m}$, with which a liquid nitrogen-cooled HgCdTe detector was used to get a high signal to noise ratio (SNR) on the recorded spectra. The measurement resolution was 0.5 cm^{-1} , to ensure the characterizing instrument lineshape function was narrow compared to that of the grating. All measurements were obtained under vacuum to reduce contribution from water vapor spectral interferences. An Allan variance measurement using these settings indicated that the optimum averaging was 40 scans, or approximately two minutes data collection at this resolution, to achieve a $\text{SNR} \approx 500$ in transmission. These settings were used across all measurements to ensure consistency. A background measurement with the grating removed was taken for each individual AOI to calculate normalized transmission and cancel angle dependent shadowing effects introduced by the aperturing mask.

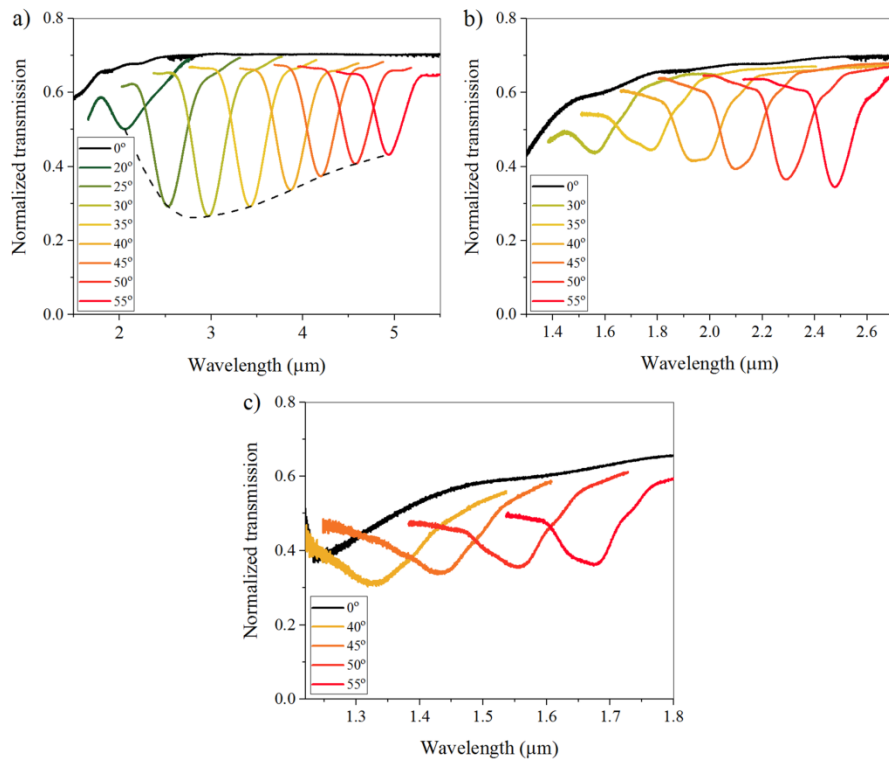


Fig. 4. Measured transmission at discrete angles of incidence. Plots are truncated to show only the first (a), second (b), or third (c) order diffraction dip. The dashed black line (a) is the superblaze of the grating, the spline is for indication only.

Measurement of the grating spectral transmission was made by adjusting the grating incident angle between 20° and 55° , at 5° intervals. A reference trace at normal incidence was also recorded. The zeroth order transmission spectrum at each discrete AOI showed evidence of first and higher order diffraction, represented as characteristic dips in the spectra. Figure 4 presents the collected spectra, truncated and split to focus only on first, second, and third order of diffraction. The grating exhibits first order diffraction at $2\text{--}5\ \mu\text{m}$ over the range of AOI tested, shown in Fig. 4(a). In this plot, the superblaze curve is materialized as a dash line. In a first approximation, the first order diffraction spectral features appear Gaussian, while the second and higher order spectra indicate additional components in the grating response function.

Peak first order diffraction efficiency for this grating is confirmed to occur at around $3\ \mu\text{m}$, where the zeroth order transmission drops from the normalized background level of 70% to 26%, a decrease of 44%. This decrease can be inferred to be the diffraction efficiency into the first diffraction order, assuming no other diffraction orders propagate at this wavelength and angle. The blaze bandwidth, calculated by fitting a Gaussian peak to the transmission curve and obtaining the full width at half-maximum (FWHM), is $0.36\ \mu\text{m}$ for the first order diffraction.

The 0° transmission curve shown in Fig. 4 relates to Fresnel reflections occurring at the IG2 plate interfaces, approximately 15% loss by reflection per interface. The short-wavelength cut-on that can be observed in the three plots of Fig. 4 relates to bulk IG2 transmission, which for a 1 mm thick disk starts to cut-off for wavelengths shorter than $1.5\ \mu\text{m}$. The FTS measurement setup also starts to cut-off at wavelengths shorter than $1.5\ \mu\text{m}$ due to source, detector, beamsplitter and window choice; this is evidenced by increased noise on the short wavelength measurements, e.g. 40° , yellow in Fig. 4(c). Addition of the above-

mentioned aperturing mask and individual background measurement yielded improved background normalization, and therefore an increase in the measured diffraction efficiency from 32% to 44%, when compared to previous measurements of the same grating [22].

As the grating response was measured across the full spectral transmission band of the material, the second and third order diffraction of the grating were also observed. In this case, lower AOI transmission falls close to the edge of the detector spectral response and could not be resolved. Figure 4(b) shows the second order data obtained for AOI between 30° and 55° , which exhibits a trend toward greater diffraction efficiency at longer wavelength. Third order diffraction has also been observed for larger AOI, as observed in Fig. 4(c). These figures also show that the higher order diffraction would enable this transmission grating to be used in a continuous spectral range from lower than $1.3 \mu\text{m}$ to $5 \mu\text{m}$, if required, and potentially at even shorter wavelengths if we were to configure the FTS to investigate these.

Transmission spectra indicate that additional lineshape function affects the grating response, particularly for higher order diffraction where the spectral response appears as a doublet. This has been observed previously [22] and is a result of imperfect collimation of the characterization source at the grating incident plane. The spectral positions of the doublet peaks can be used to determine the convergence cone angle at the air-IG2 interface using Snell's law; this was calculated to be $\text{AOI} \pm 1.35^\circ$. This effect has significant impact on the measured grating response, and is considered further in the modelling procedure.

4. Grating modelling

GSolver model

Grating modelling was performed using the G Solver modelling tool [24]. G Solver uses rigorous coupled wave analysis to obtain a numerical solution to the Maxwell equations describing the grating structure. The solver allowed the wavelength to be scanned for fixed AOI to produce simulated spectra corresponding to those experimentally measured using the FTS. The IG2 grating is modelled by defining the refractive index profile of a single grating period. A two-component grating profile was used: a higher constant refractive index ULI-modified region, and a lower constant refractive index unmodified (bulk) IG2 region. The parameters characterizing the structure were: the aspect ratio (AR), defined as the ratio of the width of the modified region to the width of a period; the grating thickness along the normal incidence optical axis; and the step refractive index modification (Δn), the difference between the refractive indices of the two components of the period. Figure 5 shows a schematic of the grating model, and definition of the model parameters.

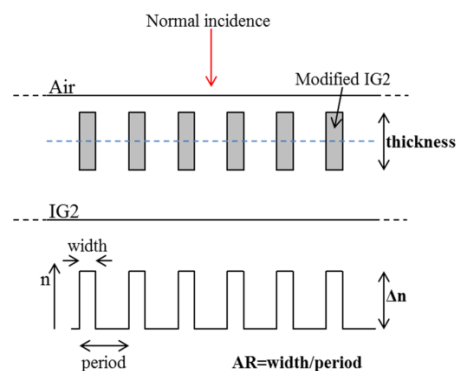


Fig. 5. Schematic of the grating structure, with definition of model parameters (bold). Refractive index profile shown (bottom) is along blue dashed line. Not to scale.

The model assumes an infinite lateral extent of the grating. In addition, by using a top-hat refractive index modulation function the ULI fabrication process is considered homogeneous

across the modified region. The spacing between the layers constituting the volume grating is also assumed small enough so that it does not affect the diffraction properties.

The fabrication characteristics could inform some of the model parameters. The grating period is 3 μm , corresponding to the air-bearing stage movement during fabrication. The number of inscribed layers (30) yields a thickness of 128 μm . Δn , and AR were derived from model optimization to the experimental data, and starting values were determined from prior modelling [22].

As the spectral dependence of refractive index of unmodified IG2 is well known across the measured band, material dispersion was included in the model using the known Sellmeier coefficients [21]. Δn was implemented as a constant increase from this Sellmeier curve; the Δn induced by ULI is considered positive and constant across 1–6 μm . The ‘grating thickness’ used in the model is the optical thickness, which therefore should have some dependence on refractive index variation across the spectral band ($\approx 4\%$ change over 1–6 μm). This proved to be difficult to implement in the model, and as such the refractive index at 3 μm ($n = 2.5181$) was chosen to maintain a constant grating thicknesses.

The modelled grating accounts only for the inscribed structure into bulk IG2. Therefore, the effect of the additional air-IG2 interfaces on both sides was added separately. Snell’s law was used to calculate the AOI in IG2 corresponding to each measurement AOI in air, and the 0° measurement shown in Fig. 4 above was used to correct for Fresnel reflection and transmission losses. Hence the model could be compared directly to the measured data.

The effect of the slightly converging illumination was also added, as it broadens the grating response function. As a first approximation, for each AOI, five spectra were modelled using AOI that were regularly spaced across the $\pm 1.35^\circ$ converging cone; the un-weighted average of these five spectra is presented in subsequent plots, unless stated otherwise.

Modelling parameter optimization

Model parameters were constrained using the following features:

- The spectral position of the minimum of the superblaze curve [25] outputted by the model was kept within $2.8 \pm 0.1 \mu\text{m}$ to match experimental data.
- The FWHM of the first order diffraction dip for each AOI on the experimental and modelled spectra were matched.
- The relative magnitude of the first, second and third diffraction orders (where available) from experimental and modelled spectra were matched for a given AOI.

The spectral position of the superblaze minima is dependent on both AR and Δn . The FWHM of the first order diffraction dip varied only with changes to the thickness parameter, with increasing thickness causing the first order diffraction dip to narrow. Similarly, the relative magnitude of the higher order diffraction dips varied only when AR was changed. Modification of AR also affects the overall shape of the superblaze curve for the first order diffraction. The relative adjustment of the modelled curve to the experimental one was found to be a robust way to derive the AR parameter. Lastly, varying Δn only affects the minima position of the superblaze curve, increasing Δn produces a shift of the minimum towards longer wavelengths.

As a result, the procedure to derive estimates from the data was as follows:

1. The relative magnitude of the second and third diffraction orders of the modelled spectra was optimized to match the experimental ones by varying the AR parameter; and so was the relative shape of the superblaze curve for the first order. This produced a shift to the superblaze curve minima.
2. The modelled superblaze curve minima was brought back within that of the experimental one by altering Δn .

This procedure yields the result shown in Fig. 6. The deduced parameter estimates were: $\Delta n = 0.031$, and $AR = 0.175$.

Figure 6(a) shows measured and modelled first order diffraction spectra using the parameter estimates. The superblaze (black dashed line) curve is well reproduced by the model, except for a near constant offset indicating an overestimation of the modelled grating efficiency of 11% across 25°–55° AOI. The difference between measured and modelled transmission reduces to 8% for second order, and 3% for third order, on average.

The effect of convergent illumination is qualitatively reproduced, especially at higher diffraction orders where it contributes significantly. However, additional contributions to the “apparatus function” broadening the spectra are apparent in the experimental data, and not reproduced by the model. Firstly, the slightly convergent illumination is crudely modelled by an aggregation of five rays that does not include beam uniformity. The large uncertainty on the illumination convergence may also play a role in this mismatch. Lastly, the nominal positioning accuracy of the translation stage is given to be 0.2 μm , which turns into potential mismatch in grating line alignment within the volume, hence adding additional broadening to the grating response function. Neither of these complex factors is understood sufficiently well to allow inclusion of a robust correction to the model and are in scope for further investigation.

Figure 6(d) shows the modelled first order diffraction expected for a perfectly collimated input beam, using the derived model parameters. The plot shows the sinc-squared spectral form expected for a top-hat refractive index modulation, which is otherwise smoothed as shown in Fig. 6(a). The theoretical FWHM is narrower and ideally the efficiency reaches almost 100% at the optimized wavelength.

At short wavelength, $< 1.5 \mu\text{m}$, for instance Fig. 6(c), 40° AOI, the modelled peak minima no longer coincide with the minima of the measured data. This is thought to indicate the difference in refractive index modification for higher orders, as described in the literature [26]. Further quantification of these effects would improve model agreement for all diffraction orders.

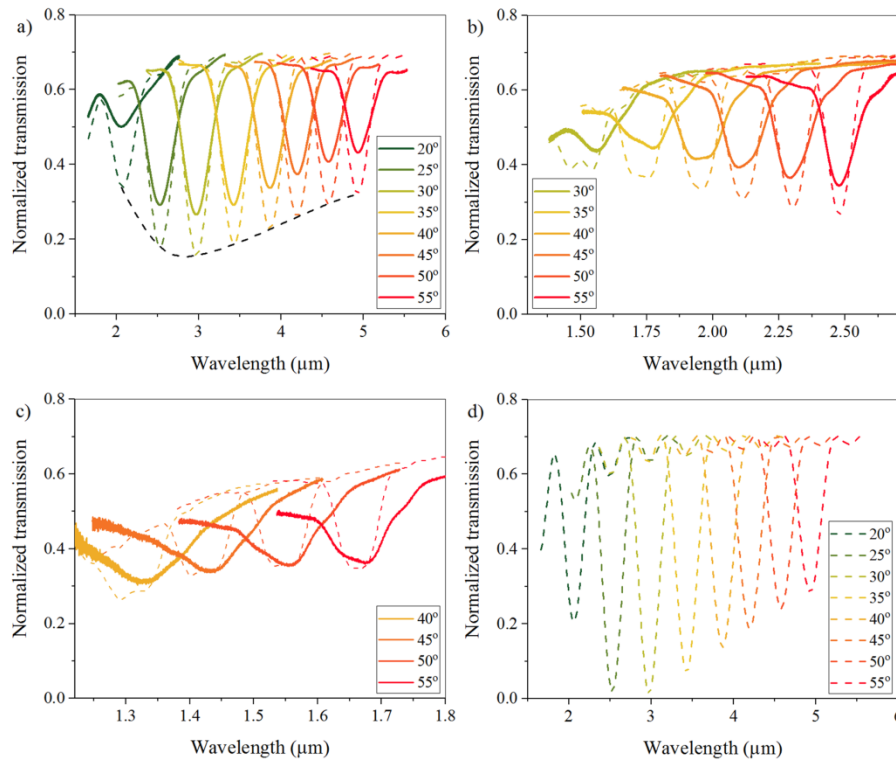


Fig. 6. Measured (bold) and modelled (dashed) spectra for changing AOI, showing the first (a), second (b), and third (c) diffraction orders. The first order modelled superblaze (dashed black) is shown (a). (d) Theoretical first order diffraction for a collimated input beam, for the same model parameters. Thickness = 128 μm , $\Delta n = 0.031$, and AR = 0.175.

Error estimation and results discussion

AR was estimated by considering both the relative diffraction efficiency of the higher order diffraction dips, and subsequently refined through superblaze curve relative adjustment. This is believed to be more robust than previous methods [22], which did not consider the higher diffraction orders. The derived $\text{AR} = 0.175 \pm 0.013$ equates to a modified refractive index region in each period approximately 0.53 μm wide. This is narrower than anticipated from the measured inscription beam dimension ($\approx 1 \mu\text{m}$) and prior modelling [19], but as the non-linear ULI procedure is related not only to physical beam size, but also to the energy distribution within the beam, this modelled value is likely to be realistic.

The $\Delta n = 0.031 \pm 0.002$ obtained with ULI in IG2 appears to be higher than anticipated, and certainly higher than that of GLS [19]. As the determination of Δn depends also on AR, the error on this estimate is expected to be ~ 0.002 ; 0.001 uncertainty propagating from the 0.013 error on AR, and 0.001 from the 0.1 μm uncertainty in the determination of the minimum of the superblaze curve position. This large Δn obtained at modest ULI fluence confirms the relevance of the IG2 material for mid IR ULI photonics devices.

5. Conclusion

ULI transmission gratings of various thicknesses were manufactured in IG2 chalcogenide glass, and demonstrated to exhibit $> 60\%$ first order diffraction efficiency from 1.4 to 2.5 μm with a limiting material transmission of 67%. From the observed linear relationship between grating thickness and peak first order diffraction wavelength, a transmission grating optimized for mid IR was developed and characterized to exhibit first order diffraction over the entire 2–5 μm infrared spectral band. The maximum first order diffraction efficiency was

at approximately $3\ \mu\text{m}$, for an AOI of 29.7° , exhibiting 44% absolute diffraction efficiency with FWHM $\approx 0.36\ \mu\text{m}$.

The grating was characterized using an FTS to measure up to the third order grating transmission spectra. These large set of experimental data, along with improvements to the modelling method, have allowed a multi-parameter analysis, beyond the Littrow method previously presented [19]. As a result, influence of the ULI fabrication parameters on the grating spectral response have been investigated and led to a more robust estimation of the volume inscribed, as well as the refractive index contrast produced in IG2.

Improved modelling and understanding of the effects of grating parameters will better inform the fabrication of future gratings, especially for devices optimized for wavelengths further into the $3\text{--}5\ \mu\text{m}$ window. The model parameter investigation suggests that gratings with larger high efficiency bandwidth (larger FWHM) would require thinner grating structures, whilst the Δn (and therefore the inscription pulse energy) ought to be adjusted to select the wavelength at which optimum efficiency is desired. Going into the mid-IR means increasing Δn , for which IG2 is demonstrated to be well suited. In addition, the superblaze curve and the grating response at higher order of diffraction can be engineered through altering the AR parameters.

The measured grating response function was found to be broadened compared to model expectation. Part of this effect was trace down to the slightly convergent illumination conditions including angular diversity to the incident beam. Additional broadening was also attributed to grating line statistical error introduced by the positioning error of the translation stages used during the inscription process. Upon successful reduction of these broadening effects, and application of an anti-reflection coating, would lead to a first order diffraction efficiency close to 97%, with FWHM $\approx 0.27\ \mu\text{m}$.

Further work to realize these improvements is on-going, as well as investigation of scattering and associated losses in ULI-modified material. Moving forward, engineering of the grating spectral response function would result in tailored grating efficiency spectra for astronomical and spectroscopic applications in the mid-IR.

Funding

Science and Technologies Facility Council (STFC) Centre for Instrumentation in Advanced Optics; STFC Consortium (ST/N000625/1).

Acknowledgment

We acknowledge the contribution of the STFC RAL Space Precision Development Facility, for design and manufacture of mounting components used for grating test in the FTS. To comply with RCUK Common Principles on Data policy, the raw data presented in this manuscript has been made available here: <http://dx.doi.org/10.5286/edata/710>.